



In vivo contact biomechanics in the trapeziometacarpal joint using finite deformation biphasic theory and mathematical modelling



Benjamin Dourthe^{a,*}, Priscilla D'Agostino^a, Filip Stockmans^{a,b}, Faes Kerkhof^a, Evie Vereecke^a

^a KU Leuven, Department of Development & Regeneration @ Kulak, Etienne Sabbelaan 53, 8500 Kortrijk, Belgium

^b AZ Groeninge, Campus Loofstraat, Loofstraat 43, 8500 Kortrijk, Belgium

ARTICLE INFO

Article history:

Received 6 March 2015

Revised 11 September 2015

Accepted 3 November 2015

Keywords:

Biomechanics

Trapeziometacarpal joint

TMC joint

Mathematical modelling

Contact patterns

in vivo

Medical imaging

Cartilage

Osteoarthritis

ABSTRACT

The assessment of the contact biomechanics in the trapeziometacarpal (TMC) joint during functional tasks represents a relevant way to obtain a better understanding of the onset of osteoarthritis (OA). CT scans of the hand region of 20 female volunteers were taken in relaxed neutral, lateral key pinch and power grasp configuration. 3D models of the first metacarpal (MC1) and the trapezium were created. The articular area of each bone was quantified and a mathematical model was developed in Matlab to evaluate the projected contact area and stress distribution of each bone. The articular areas of the MC1 and the trapezium presented no significant difference. A slightly smaller projected contact area was calculated for the trapezium compared to the MC1. Similar amounts of stress were reported in the neutral and lateral pinch configurations. The highest stress levels were observed during power grasp. Very consistent results for high stress location on the volar/radial articular sub-region were found in the neutral and power grasp configurations. More variation was reported during lateral pinch. The mathematical model presented in this paper offers the possibility to predict contact patterns within the TMC joint based on *in vivo* CT images.

© 2015 IPEM. Published by Elsevier Ltd. All rights reserved.

1. Introduction

Osteoarthritis (OA) is a degenerative joint disease characterized by the loss of the articular cartilage which leads to joint pain and decrease in mobility [1]. It represents the most common type of arthritis [2] and a chronic disability which primarily affects the middle-aged and elderly population with a fast increasing prevalence with aging [3]. Osteoarthritis cannot be cured, but the symptoms can be relieved by conservative and/or surgical treatment (e.g. NSAIDs, splinting, joint replacement). However, OA remains a complex disabling disease which cause is not completely understood and further investigation is required to find more effective prevention and treatment strategies for early stages of the disease.

The human trapeziometacarpal (TMC) joint has been described as a concavo-convex joint with two non-orthogonal axes of rotation allowing abduction–adduction, extension–flexion and axial rotation [4–6]. Together with the well-developed thenar musculature and the relatively long thumb length, this gives the human thumb the high mobility that is responsible for the unique dexterity of modern humans. However, this high joint mobility also makes the joint particularly prone to pathologies, such as OA. The TMC joint has been

reported as the most common location for development of OA in the hand [7]. Important mechanical factors which have been identified as being linked to the development of OA are joint instability [8] and lack of joint congruence [9]. Both factors will lead to peak loading, which will further accelerate the development of OA.

The physical characteristics of the cartilage, such as its thickness or integrity, can be largely affected by wear patterns induced by high amounts of stress. Pinching and gripping represent two crucial tasks in daily activities. These two different actions allow us to perform important tasks such as writing or holding objects of various shapes, and allow us to manipulate them with a combination of precision and strength. Cooney and Chao [10] reported an average compressive force within the TMC joint of 12 kg, and up to 120 kg during a strong grip. These represent high values for a non-weight-bearing joint of that size. This also indicates a need for stability in the TMC joint in order to withstand high compressive forces in these specific positions.

Very few models of the TMC joint have been developed to calculate the contact patterns occurring during daily manual activities. The purpose of this study is to estimate the change in the contact stress distribution in the TMC joint from a relaxed neutral position to submaximal (80% of the maximal strength) lateral key pinch and power grasp. We expect that regions of high contact stress will correspond to wear patterns of the cartilage in the arthritic TMC joint. With this study, we aim to develop a 3D mathematical model allowing

* Corresponding author. Tel.: +32 56 24 64 94.

E-mail address: benjamin.dourthe@kuleuven-kulak.be, b.dourthe@hotmail.fr (B. Dourthe).



Fig. 1. Photos of the three different scanning configurations: (a) relaxed neutral; (b) lateral key pinch; (c) power grasp.

Table 1
Scanning parameters.

Slice thickness	Pixel size	FOV	Voltage	Source current	Scanning algorithm
0.625 mm	0.293 mm	150 mm	100 kV	156 mA	Bone

investigations of the biomechanical behaviour of the TMC joint, without the need for invasive techniques. Such insight could eventually contribute to better prevention and treatment strategies for TMC OA.

2. Materials and Methods

2.1. Subject selection

After permission by the Medical Ethical Commission of the University of Leuven (Belgium, #B322201420166), 20 female volunteers (mean age: 60.8 years; range, 50–82 years; 17 right-handed, 3 left-handed) were recruited to participate in the study. Each subject signed an informed consent prior to the start of the study. Each volunteer underwent a clinical examination of both hands by a professional hand surgeon (PDA) in order to determine the dominant hand and to confirm the absence of TMC OA according to RX images. The dominant hand was defined as the hand showing the greatest strength during lateral pinch and power grasp force measurements. Four patients showed radiological signs of early or late stage of OA and were excluded from the study.

2.2. Scanning protocol

Each subject's dominant hand was scanned using a 64 slice Discovery HD 750 CT scanner (GE Healthcare, Little Chalfont, United Kingdom) at the hospital AZ Groeninge, Belgium. The scanning parameters are listed in Table 1.

The hand region of each subject was scanned from the distal part of the radius to the first metacarpophalangeal joint in three different configurations:

- *Relaxed neutral*: a neutral position splint (RolyanOriginal; Patterson Medical, Bolingbrook, IL, USA) placed the wrist in a relaxed neutral anatomic posture as shown in Fig. 1a.
- *Lateral key pinch*: the patient was holding a compression load cell (0–50 pounds [0–22.7 kg]; Model D Thu-Hole Load Cell; Honeywell International Inc., Morristown, NJ, USA) between the thumb and the index finger as shown in Fig. 1b. Each patient was asked to apply a submaximal force of 80% of their maximal pinch force by following the measurement on a screen. Specific attention was made to avoid motion artefacts while scanning.
- *Power grasp*: the patient was holding a cylinder equipped with the same load cell previously used for the lateral key pinch (Fig. 1c).

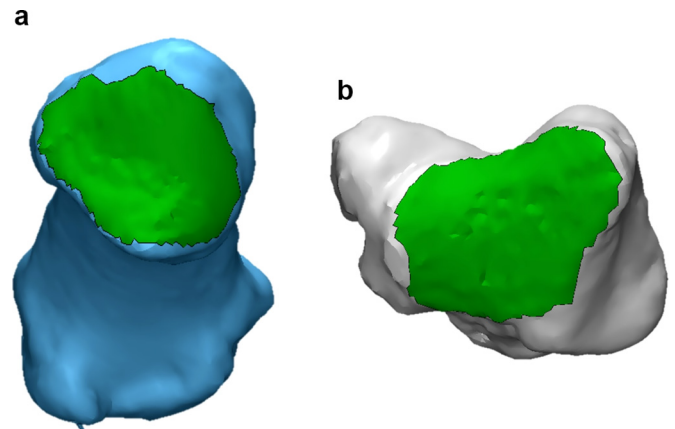


Fig. 2. Manual measurement of the articular area (in green) of (a) MC1 and (b) trapezium of the right hand of one subject. (For interpretation of the references to colour in this figure legend, the reader is referred to the web version of this article.)

Each scan was performed while applying a submaximal force corresponding to 80% of the maximal grip strength.

2.3. Image segmentation

Each scan was reconstructed in a DICOM format and segmented semi-automatically using medical image processing software (Mimics Research 17.0 × 64 with CT bone plug-in, Materialise, Leuven, Belgium) with constant segmentation parameters (thresholding: min. of 294 Hounsfield - smoothing: 1 iteration, smooth factor of 0.4). Separate 3D surface models of the first metacarpal (MC1) and the trapezium were reconstructed for further data analysis.

The articular area was measured manually by following the border of the articular surface for each bone (Fig. 2) in the neutral configuration using an anatomical CAD software (3-matic Research 9.0 × 64, Materialise, Leuven, Belgium). To avoid subjective bias, two observers independently performed a series of five measurements for each articular area. Each measurement was reported in table format (Table 2) and the average and standard deviation were calculated. We also calculated the operator error, i.e. the average standard deviation of each set of five measurements.

2.4. Mathematical model

A mathematical model was designed in Matlab (v. R2014a x64, MathWorks, Inc.) to estimate the contact stress distribution in the TMC joint. This code was based on the finite deformation biphasic theory developed by Kwan et al. [11]. The theory includes the effects of non-linear material properties such as permeability and solid-to-fluid volumetric ratio (expression (1)). The finite deformation biphasic theory has been shown as the most accurate way to describe the

Table 2

Average articular areas of the MC1 and trapezium measured by two observers, including the average operator error and the average between the two observers.

Bone	Parameter	Observer #1	Observer #2	Average between observers
MC1	Average articular area	135.95 mm ² ± 10.79 mm ²	133.21 mm ² ± 10.76 mm ²	134.58 mm ² ± 10.78 mm ²
	Average operator error	1.70 mm ² ± 0.54 mm ²	1.70 mm ² ± 0.82 mm ²	1.70 mm ² ± 0.68 mm ²
Trapezium	Average articular area	129.05 mm ² ± 13.06 mm ²	126.78 mm ² ± 14.86 mm ²	127.92 mm ² ± 13.96 mm ²
	Average operator error	1.71 mm ² ± 0.75 mm ²	1.71 mm ² ± 0.91 mm ²	1.71 mm ² ± 0.83 mm ²

biomechanical behaviour of cartilage under slow strain and infinitesimal strain rate conditions [11]. This theory relies on cartilage biomechanical properties and cartilage deformation.

$$\sigma = \frac{1}{4}H_A[1 + d_1(\lambda - 1)]\frac{1}{\lambda}\left(\lambda^2 - \frac{1}{\lambda^2}\right) \quad (1)$$

With:

- σ : contact stress (MPa)
- H_A : aggregate modulus (MPa)
- λ : stretch ratio in the direction of the compressive load
- d_1 : cartilage property

The aggregate modulus is a function of Lamé's parameters, as shown in expression (2):

$$H_A = \lambda_s + 2\mu_s \quad (2)$$

The cartilage property d_1 is a function of two material properties, as shown in expression (3):

$$d_1 = \frac{d_0(\alpha_0 + 1)}{d_0 + \alpha_0} \quad (3)$$

with

- d_0 : fluid-to-solid true density ratio,
- α_0 : initial solid content.

Since the protocol followed did not allow to perform mechanical tests to estimate subject-specific cartilage properties, we used average values obtained from cadaveric studies found in the literature [11–13]. Kwan et al. [11] performed a series of test on human knee cartilage, and found an average aggregate modulus of 0.563 ± 0.272 MPa. They used an average value for α_0 of 0.20 and noted that the value of d_0 was estimated between 0.70 and 0.90, depending on cartilage chemical composition. For the mathematical model used in this study, we chose the following cartilage properties values, based on values presented in the literature: $H_A = 0.8$ MPa, $\alpha_0 = 0.20$ and $d_0 = 0.90$. The chosen value of the aggregate modulus also corresponds to the range of equilibrium compressive modulus of adult articular cartilage reported by Buckwalter et al. [13].

The cartilage strain was evaluated by creating a uniform cartilage layer over each bone, covering the articular area with a constant thickness along the joint surface (Fig. 3). Koff et al. [12] measured the average cartilage thickness for the trapezium and MC1 by using stereophotogrammetry of 104 fresh-frozen thumbs diagnosed with different stages of OA, among which 44 specimens were categorized as normal joints with smooth and intact surfaces. They obtained a surface-wide mean thickness of the articular layer of 0.8 ± 0.2 mm for the trapezium and 0.7 ± 0.2 mm for the MC1 in non-arthritic joints. Seen the large sample size and consistent methodology, we used these values in our model.

The minimal distance between two neighbouring points located on the surface of each bone was calculated as shown in Fig. 3.

Expression (4) was used in order to calculate the total cartilage deformation:

$$\varepsilon_t = (T_{MC1} + T_{trap}) - d_{min} \quad (4)$$

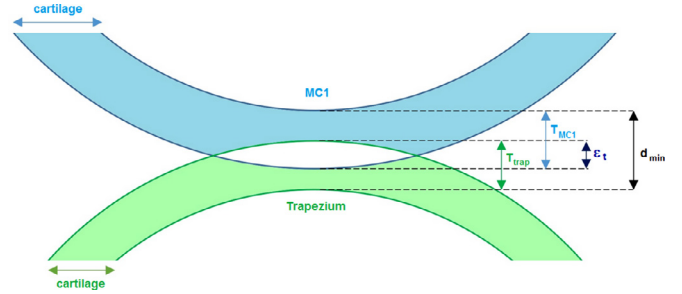


Fig. 3. Scheme representing the elastic deformation zone of the cartilage (T_{trap} : cartilage thickness of the trapezium; T_{MC1} : cartilage thickness of the MC1; ε_t : cartilage deformation; d_{min} : minimal distance between two neighbouring points from each bone).

With:

- T_{MC1} : cartilage thickness of MC1 (mm)
- T_{trap} : cartilage thickness of the trapezium (mm)
- d_{min} : minimal distance between two neighbouring points from each bone (mm)

As each cartilage layer was considered to have the same mechanical properties, we took the assumption that the deformation was equally distributed between each layer. Expression (5) represents the corresponding deformation for each cartilage layer:

$$\varepsilon_{MC1} = \varepsilon_{trap} = \frac{\varepsilon_t}{2} = \Delta l \quad (5)$$

The Cauchy strain was calculated as a ratio between the deformation and the original thickness of each cartilage layer as shown in expressions (6) and (7):

$$e_{MC1} = \frac{\varepsilon_{MC1}}{T_{MC1}} = \frac{\Delta l}{L_1} = \frac{l_1 - L_1}{L_1} \quad (6)$$

$$e_{trap} = \frac{\varepsilon_{trap}}{T_{trap}} = \frac{\Delta l}{L_2} = \frac{l_2 - L_2}{L_2} \quad (7)$$

with

- l_i : final thickness of the i th component (1 for MC1 and 2 for the trapezium),
- L_i : original thickness of the i th component.

The stretch ratio, corresponding to the ratio between the final and the original cartilage thicknesses, was calculated using expression (8) and (9) for each cartilage layer:

$$\lambda_{MC1} = \frac{l_1}{L_1} = e_{MC1} + 1 \quad (8)$$

$$\lambda_{trap} = \frac{l_2}{L_2} = e_{trap} + 1 \quad (9)$$

The contact stress was calculated for each cartilage layer as a function of the corresponding stretch ratio (see expression (1) from Kwan et al. [11]) and for each couple of neighbouring points located in the deformation area ($\varepsilon_t > 0$). The contact stress values obtained for each

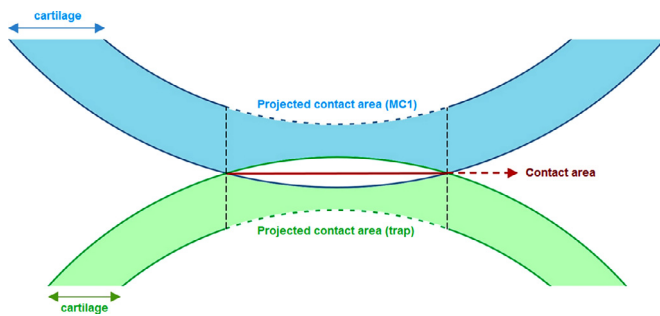


Fig. 4. Scheme representing the contact area (in red) between the MC1 and the trapezium and the two corresponding projected contact areas. (For interpretation of the references to colour in this figure legend, the reader is referred to the web version of this article.)

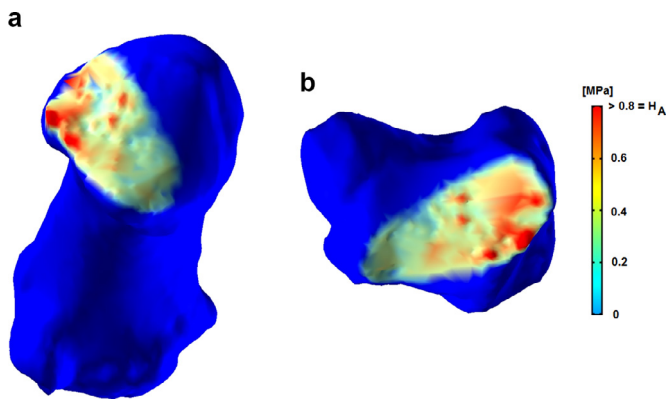


Fig. 5. 3D model of the MC1 (a) and the trapezium (b) of the right hand of a subject showing the stress distribution predicted by the model (H_A : aggregate modulus of the cartilage).

bone were added to obtain the total contact stress, as shown by expression (10):

$$\sigma_t = \sigma_{MC1} + \sigma_{trap} \quad (10)$$

Two different stress values were given as output: the *maximum* contact stress (σ_{max}) and the *average* contact stress (σ_{av}) which corresponds to the average of all the stress values calculated for each point located in the deformation area.

Another parameter, called the *projected contact area*, was estimated using the same Matlab code. The term 'projected' refers to the fact that the points selected for area calculation are located on the articular surface of each bone. This area was obtained by adding the areas of the triangles created by the different points allocated to the deformation area. An illustration of this parameter is shown on Fig. 4. Each projected contact area was displayed on the 3D model of the corresponding bone with a colour code indicating the stress distribution (Fig. 5). Next, we calculated the *area ratio*, i.e., the ratio between the projected contact area and the articular area, for each bone and each task to account for inter-individual differences in bone size.

2.5. Articular surface division

In order to interpret the stress distribution results obtained through mathematical modelling, we divided the articular surfaces of the MC1 and the trapezium in nine sub-regions, as shown in Fig. 6. The colour maps representing the contact patterns were carefully assessed in order to evaluate the most stressed sub-region for each configuration. For each subject, each time a stressed zone was observed in one sub-region, one was added to the corresponding stress counter. Note that in order to avoid any confusion between right and left hand,

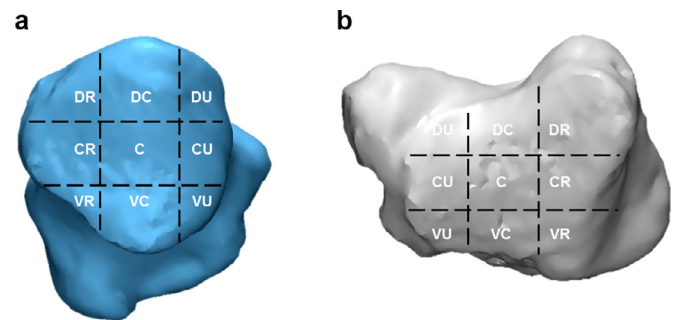


Fig. 6. Sub-divisions of the articular surface of MC1 (a) and trapezium (b) of the right hand of one subject (DR: dorsal-radial; DC: dorsal-central; DU: dorsal-ulnar; CR: central-radial; C: central; CU: central-ulnar; VR: volar-radial; VC: volar-central; VU: volar-ulnar).

each left hand model ($n = 3$) was mirrored before performing the stress location classification.

2.6. Statistical analysis

Statistical analysis was performed in Excel for Windows (Microsoft, Redmond, WA, USA). A Student's *t*-test was used to test if the projected contact areas and area ratios of the trapezium were significantly different than those of MC1, for each isometric task separately (one-tailed distribution, two-sample equal variance/homoscedastic). To compare the projected contact area, area ratio and contact stress differences between tasks, we used different function parameters (two-tailed distribution, paired values). A *p*-value inferior to 0.05 was considered as statistically significant.

3. Results

3.1. Articular area, projected contact area and area ratio

The average articular area of MC1 amounted to $134.58 \pm 10.78 \text{ mm}^2$ (average \pm standard deviation) and $127.92 \pm 13.96 \text{ mm}^2$ for the trapezium, as shown in Table 2. No statistical difference was found between the articular areas of the two bones ($p > 0.05$).

The projected contact area (PCA) of each bone was calculated in each of the three different configurations (see Table 3). No significant difference in projected contact area was reported between tasks neither for the MC1 nor for the trapezium ($p > 0.1$). However, for each task, we observed a slightly smaller projected contact area for the trapezium compared with the MC1. This result was only statistically significant in the lateral key pinch configuration (neutral: $p = 0.05$; lateral key pinch: $p < 0.05$; power grasp: $p = 0.07$).

No statistical difference was observed for the area ratio of each bone between tasks ($p > 0.1$). The area ratio of the MC1 was higher than for the trapezium in the neutral and lateral key pinch configuration, but not statistically significant (neutral: $p = 0.077$; lateral key pinch: $p = 0.054$). No statistical difference between area ratio of MC1 and trapezium during power grasp was observed ($p > 0.1$).

3.2. Contact stress calculation

The maximum contact stress is calculated at the points where the distance between the MC1 and the trapezium is the smallest. The minimum inter-bone distance and the maximum and average contact stress values obtained by mathematical modelling are listed in Table 4. The results corresponding to the neutral position and the lateral key pinch are very similar (σ_{max} and σ_{av} : $p > 0.1$). The contact stress calculated during power grasp is significantly higher compared to that of the two other configurations ($p < 0.05$), with an average

Table 3

Calculated projected contact areas (PCA) and area ratios of the MC1 and the trapezium in three different configurations (average \pm standard deviation).

Configuration	Neutral	Lateral pinch	Power grasp
PCA (MC1)	36.43 mm ² \pm 19.49 mm ²	40.97 mm ² \pm 20.21 mm ²	35.92 mm ² \pm 13.03 mm ²
PCA (Trapezium)	26.12 mm ² \pm 14.00 mm ²	28.75 mm ² \pm 11.74 mm ²	29.28 mm ² \pm 10.95 mm ²
Area ratio (MC1)	27% \pm 15%	31% \pm 15%	27% \pm 10%
Area ratio (Trapezium)	21% \pm 11%	23% \pm 10%	23% \pm 9%

Table 4

Minimum inter-bone distance, maximum and average contact stress calculation in three different configuration (average \pm standard deviation).

Configuration	Neutral	Lateral pinch	Power grasp
Minimum inter-bone distance	0.86 mm \pm 0.21 mm	0.85 mm \pm 0.16 mm	0.58 mm \pm 0.19 mm
Maximum contact stress	0.62 MPa \pm 0.20 MPa	0.63 MPa \pm 0.15 MPa	0.89 MPa \pm 0.18 MPa
Average contact stress	0.16 MPa \pm 0.04 MPa	0.17 MPa \pm 0.04 MPa	0.24 MPa \pm 0.04 MPa

increase from neutral to power grasp of 0.27 MPa \pm 0.18 for σ_{max} , and 0.08 MPa \pm 0.04 for σ_{av} .

3.3. Stress distribution

The stress distribution observed for each bone in each configuration is shown in Table 5. Consistent contact patterns are found, especially for the neutral position (dominant: volar-central) and the power grasp (dominant: radial) with almost no variation between subjects. More variation is observed for lateral key pinch (dominant: volar-central).

4. Discussion

In this study, we developed a 3D mathematical model to evaluate the contact biomechanics of the TMC joint during specific functional tasks. The model is based on a mathematical definition of the biomechanical behaviour of the cartilage [11] using mechanical properties taken from the literature [11–13]. In the past decades, *in vitro* techniques, such as the casting method [14], pressure sensor sheet [15,16] or cartilage staining techniques [17] have been used to measure intra-articular contact area. More recently, super-low-pressure-sensitive film has been used to measure the pressure distribution in small non-weight-bearing joints like the wrist [18–20] and the thumb joint [21]. While these studies have provided important information on joint loading, the applied methods have in common that they are highly invasive and can only be used in cadaver studies. The big advantage of the model we present in this paper is that it relies mainly on medical imaging techniques, which are easily applicable *in vivo* and in a clinical context.

The insights of our computational method showed many interesting points of comparison with the results obtained through non-numerical techniques presented in the literature. Momose et al. [22] found, using a casting method, a mean area ratio of 28.0% \pm 9.1 for the MC1 and of 27.7% \pm 6.2 for the trapezium during thumb abduction. These results correspond to our findings in the power grasp configuration – 27% \pm 10 for MC1 and 23% \pm 9 for the trapezium – where the thumb position is similar, indicating that only a third of the articular surface is loaded during power grasp. The average articular area reported by Kovler et al. [23] was 184 mm² and 160 mm² for the MC1 and the trapezium respectively. Those results are slightly higher than ours, and display a small difference between the MC1 and the trapezium. However, we note that the articular area is highly dependent on subject-specific characteristics, such as size, weight and sex. Our study only included female subjects ($n = 16$), while Kovler et al. [23] analysed a majority of male subjects (15 males, 10 females), which might explain the difference between results.

We observed a small difference between the projected contact areas of the MC1 and the trapezium, which was statistically significant in the lateral key pinch position ($p < 0.05$), but not for the two other configurations (neutral: $p = 0.05$; power grasp: $p = 0.07$). This difference can be explained by the fact that these areas are projections of the 2D deformation area on the articular surface, which is unique to each bone. Thus, more irregularities on the articular surface of one bone will result in a larger projected contact area. This indicates that the articular surface of the MC1 has more irregularities than the trapezium. Since the amount of stress is the same for the whole joint, a smaller projected contact area might show that the trapezium is subjected to stress concentration. This suggests that the cartilage layer of the trapezium is more prone to degenerative changes than the MC1, leading to an initial wear of the articular surface of the trapezium, as reported by Pellegrini [24], who observed a greater articular area eburnation on the trapezium than on the MC1, with a ratio of nearly 3:1. Such insight can be of interest for clinicians who are trying to understand and predict the occurrence mechanisms and primary location of early degenerative changes in the TMC joint.

The quantification of intra-articular contact stress shows that a similar amount of stress arises in the neutral and lateral key pinch positions (σ_{max} and σ_{av} : $p > 0.1$), while a higher stress is calculated in the power grasp configuration. A comparable difference in joint loading between lateral pinch and power grasp has been reported by Cooney and Chao [10], who found contact forces ranging from 9.33 to 13.40 kg in the lateral key pinch configuration with 1 kg of applied force, while contact forces during power grasp with 10 kg of applied force ranged from 85.4 to 164.2 kg. The calculation of a similar amount of stress for the neutral position and the lateral key pinch is surprising as the neutral position is not loaded compared to the lateral key pinch. A possible explanation for this observation is that the orientation of the thumb in both configurations is comparable. This could be assessed in a follow-up study, with additional information on muscle and joint contact forces and by using a musculoskeletal model of the TMC joint.

In terms of stress location, we observed consistent patterns across subjects in the neutral and power grasp configurations. Most of the contact pressure arises around the volar-central aspect of the articular surface in the neutral position, and around the radial sub-region during power grasp. During lateral key pinch, contact patterns are slightly less consistent across subjects, but the volar-central side remains prevailing. This lack of consistency during lateral key pinch might result from the low reproducibility of this task. It might also indicate a higher level of joint instability in this specific configuration. The consistent stress distribution pattern predicted by our model during power grasp is in agreement with the wear patterns

Table 5Stress counters representing the stress distribution for each bone in three different configurations for all subjects ($n = 16$).

Articular sub-region		Dorsal			Central			Volar		
		Radial	Central	Ulnar	Radial	Central	Ulnar	Radial	Central	Ulnar
Neutral	MC1	1	0	0	2	1	1	2	11	0
	Trap	2	0	0	2	1	1	4	9	0
Lateral key pinch	MC1	3	0	0	2	0	1	3	8	2
	Trap	3	0	0	2	1	1	1	7	4
Power grasp	MC1	7	0	0	5	1	0	3	1	1
	Trap	6	1	0	7	3	1	1	1	1

observed in arthritic TMC joints by Kovler et al. [23] and Momose [25]. Both reported the radial aspect of the joint as the most degenerated region for samples with different stages of OA. This finding is also supported by Van Nortwick et al. [26] who reported a dominant wear pattern on the radial and volar sides of trapezium bones with saddle morphology. These insights remain, however, contested. Pellegrini [27] reported that cartilage degeneration occurs on the volar-ulnar side of MC1 and the volar-central aspect of the trapezium in the first stages of OA. In a pilot study, Goto et al. [28] also observed a volar-central dominant contact pattern during thumb circumduction with one healthy subject, which remains in agreement with our current findings in the neutral and lateral key pinch configurations. In contrast, Kovler et al. [23] pointed to the dorsal-radial side of the trapezium of healthy to highly arthritic cadaveric specimens as the most affected region. This was also supported by Koff et al. [12], who added that degenerative changes progressed to the volar aspect of the trapezium in later stages of TMC OA. This lack of consistent reports supports the need for more investigations on intra-articular stress distribution and more *in vivo* studies. Next to experimental methods allowing assessment of intra-articular stress, we advocate that modelling techniques are keys to improve our understanding of joint function and loading.

The aim of this study was to develop a mathematical model enabling the prediction of *in vivo* pressure distribution in the TMC joint. While the contact stress patterns predicted by our model are consistent with what is expected for a non-weight bearing joint at this location, an improvement of accuracy could possibly be obtained by using subject-specific cartilage parameters. The average cartilage properties used in this study were obtained from knee cartilage, due to the lack of accurate data of thumb cartilage. Recent studies performed by Afara et al. [29–31] presented a new non-destructive and non-invasive method to evaluate articular cartilage mechanical properties using near-infrared spectroscopy, which could be explored in future modelling studies. We note that our findings are highly dependent on inter-bones distances. Thus, we have to take into account that the segmentation error, which is inherently present when working with medical images, might affect the geometry of the 3D bone models, which on its turn might affect the inter-bones distance. Van den Broeck et al. [32] estimated the segmentation error of CT-based 3D reconstructions to a RMS error of 0.55 mm by using similar scanning parameters. Knowing that the smallest range of inter-bones distances is 0.58 ± 0.19 mm during power grasp, the segmentation error cannot be neglected. In future work, more accurate scanning techniques, such as Cone Beam CT, will be explored to increase the scanning resolution and to decrease the segmentation error for more accurate results.

Despite these limitations, our model gives consistent predictions of stress distribution in the TMC joint during different functional activities. Validation remains complicated due to a lack of available contact stress data and *in vivo* assessment techniques for the TMC joint. We believe that this model offers an important possibility to investigate *in vivo* joint contact patterns and joint loading for not

only the TMC joint but also any other joint. In conclusion, we believe this model will contribute to a better understanding of TMC joint function in the early onset of osteoarthritis, and eventually improve prevention and treatment strategies of this highly disabling disease.

Conflict of interests

The authors declare that there is no conflict of interests regarding the publication of this paper. Ethical approval was obtained on the 12/03/2014 from the Medical Ethical Committee of KU Leuven/UZ Leuven prior to initiation of data collection (Reference number: B322201420166).

Acknowledgements

The author wishes to thank Dr. Eddy Brugman and the technical staff of the Medical Imaging department of the AZ Groeninge (Kortrijk, Belgium) for their contribution to this study. Funding for this study was obtained via the Materialise-Kulak Chair for Hand Surgery granted by the company Materialise (Leuven, Belgium).

References

- [1] Woolf AD, Pfleger B. Burden of major musculoskeletal conditions. *Bull World Health Organ* 2003;81(9):646–56.
- [2] National Collaborating Centre for Chronic Conditions Osteoarthritis: national clinical guideline for care and management in adults. London, UK: Royal College of Physicians; 2008.
- [3] Peterson IF. Occurrence of osteoarthritis of the peripheral joints in European population. *Ann Rheum Dis* 1996;55(9):659–61.
- [4] Hollister A, Buford W, Myers L, Giurintano D, Novick A. The axes of rotation of the thumb carpometacarpal joint. *J Orthop Res* 1992;10(3):454–60.
- [5] Domalain MF, Seitz WH, Evans PJ, Li Z. Biomechanical effect of increasing or decreasing degrees of freedom for surgery of trapeziometacarpal joint arthritis: a simulation study. *J Orthop Res* 2011;29(11):1675–81.
- [6] Chèze L, Dumas R, Comtet JJ, Rumelhart C, Fayet M. Determination of the number of degrees of freedom of the trapeziometacarpal joint-an *in vitro* study. *IRBM* 2012;33(4):272–7.
- [7] Marshall M, Van der Windt D, Nicholls E, Myers H, Dziedzic K. Radiographic thumb osteoarthritis: frequency, patterns and associations with pain and clinical assessment findings in a community-dwelling population. *Rheumatology (Oxford)* 2011;50(4):735–9.
- [8] Jónsson H, Valtýsdóttir STH, Kjartansson Ó, Brekkan Á. Hypermobility associated with osteoarthritis of the thumb base: a clinical and radiological subset of hand osteoarthritis. *Ann Rheum Dis* 1996;55(8):540–3.
- [9] Conconi M, Halilaj E, Castelli VP, Crisco JJ. Is early osteoarthritis associated with differences in joint congruence? *J Biomech* 2014;47(16):3787–93.
- [10] Cooney WP III, Chao EYS. Biomechanical analysis of static forces in the thumb during hand function. *J Bone Joint Surg Am*; 59(1):27–36.
- [11] Kwan MK, Lai WM, Mow VC. A finite deformation theory for cartilage and other soft hydrated connective tissues-I. Equilibrium results. *J Biomech* 1990;23(2):145–55.
- [12] Koff MF, Ugwonalu OF, Strauch RJ, Rosenwasser MP, Ateshian GA, Mow VC. Sequential wear patterns of the articular cartilage of the thumb carpometacarpal joint in osteoarthritis. *J Hand Surg Am* 2003;28(4):597–604.
- [13] Buckwalter JA, Mankin HJ, Grodzinsky AJ. Articular cartilage and osteoarthritis. *Instr Course Lect* 2005;54:465–80.

- [14] Stormont TJ, Morrey BF, Chao EY. Elbow joint contact study: comparison of techniques. *J Biomech* 1985;18(5):329–36.
- [15] Fukubayashi T, Kurosawa H. The contact area and pressure distribution pattern of the knee: a study of normal and osteoarthritic knee joints. *Acta Orthop Scand* 1980;51(6):871–9.
- [16] Pellegrini VD, Olcott CW, Hollenberg G. Contact patterns in the trapeziometacarpal joint: the role of the palmar beak ligament. *J Hand Surg Am* 1993;18(2):238–44.
- [17] Black JD, Matejczyk MB, Greenwald AS. Reversible cartilage staining technique for defining articular weight-bearing surfaces. *Clin Orthop Relat Res* 1981(159):265–7.
- [18] Hogan CJ, McKay PL, Degnan GG. Changes in radiocarpal loading characteristics after proximal row carpectomy. *J Hand Surg Am* 2004;29(6):1109–13.
- [19] Tang P, Gauvin J, Muriuki M, Pfaeffle JH, Imbriglia JE, Goitz RJ. Comparison of the “contact biomechanics” of the intact and proximal row carpectomy wrist. *J Hand Surg Am* 2009;34(4):660–70.
- [20] Zhu YL, Xu YQ, Ding J, Li J, Chen B, Ouyang YF. Biomechanics of the wrist after proximal row carpectomy in cadavers. *J Hand Surg Eur Vol* 2010;35(1):43–5.
- [21] Moulton MJ, Parentis MA, Kelly MJ, Jacobs C, Naidu SH, Pellegrini VD. Influence of metacarpophalangeal joint position on basal joint-loading in the thumb. *J Bone Joint Surg Am* 2001;83-A(5):709–16.
- [22] Momose T, Nakatsuchi Y, Saitoh S. Contact area of the trapeziometacarpal joint. *J Hand Surg Am* 1999;24(3):491–5.
- [23] Kovler M, Lundon K, McKee N, Agur A. The human first carpometacarpal joint: osteoarthritic degeneration in 3-dimensional modeling. *J Hand Ther* 2004;17(4):393–400.
- [24] Pellegrini VD. Osteoarthritis of the trapeziometacarpal joint: the pathophysiology of articular cartilage degeneration. II. Articular wear patterns in osteoarthritic joint. *J Hand Surg Am* 1991;16(6):975–82.
- [25] Momose T. Cartilage degeneration and measurement of the contact area of the trapeziometacarpal joint: morphological observation. *Nihon Seikeigeka Gakkai Zasshi* 1994;68(5):426–34.
- [26] Van Nortwick S, Berger A, Cheng R, Lee J, Ladd AL. Trapezial topography in thumb carpometacarpal arthritis. *J Wrist Surg* 2013;2(3):263–70.
- [27] Pellegrini VD. Osteoarthritis of the trapeziometacarpal joint: the pathophysiology of articular cartilage degeneration. I. Anatomy and pathology of the aging joint. *J Hand Surg Am* 1991;16(6):967–74.
- [28] Goto A, Leng S, Sugamoto K, Cooney WP, Kakar S, Zhao L. In vivo pilot study evaluating the thumb carpometacarpal joint during circumduction. *Clin Orthop Relat Res* 2014;472(4):1106–13.
- [29] Afara I, Prasadam I, Crawford R, Xiao Y, Oloyede A. Non-destructive evaluation of articular cartilage defects using near-infrared (NIR) spectroscopy in osteoarthritic rat models and its direct relation to Mankin score. *Osteoarthr Cartil* 2012;20(11):1367–73.
- [30] Afara I, Singh S, Oloyede A. Application of near infrared (NIR) spectroscopy for determining the thickness of articular cartilage. *Med Eng Phys* 2013;35(1):88–95.
- [31] Afara I, Singh S, Oloyede A. Load-unloading response of intact and artificially degraded articular cartilage correlated with near infrared (NIR) absorption spectra. *J Mech Behav Biomed Mater* 2013;20:249–58.
- [32] Van den Broeck J, Vereecke E, Wirix-Speetjens R, Vander Sloten J. Segmentation accuracy of long bones. *Med Eng Phys* 2014;36(7):949–53.